Use of low-cost accelerometers for landslides monitoring: results from a flume experiment

Malena D'Elia Otero[1]# [iD], Ana Elisa Silva de Abreu[1] [iD], Amin Askarinejad[2] [iD],

Marcela Penha Pereira Guimarães[3] [iD], Eduardo Soares de Macedo[3] [iD],

Alessandra Cristina Corsi[3] [iD], Rynaldo Zanotele Hemerly de Almeida[3] [iD]

Article

Abstract

Early Warning Systems (EWS) are non-structural measures for landslides disaster prevention. They are based on the detection of impending failure signals. The results of a landslide simulation experiment where accelerometers were used to identify pre-failure signals are presented in this paper. Landslide was simulated in a tilting flume filled with sandy soil. During the experiment, the flume was fixed at 30° inclination and water percolated through the soil until it slid. Accelerometers were embedded into the soil and recorded acceleration data from the beginning of the experiment until failure. Acceleration data were analyzed in time domain aiming at estimating translational velocity of the movement. Angular variation was also estimated from acceleration data. The experiment was recorded with a camera and pictures were used for Particle Image Velocimetry (PIV) analysis, in order to validate the estimated translational velocity. Results showed that accelerometers can identify pre-failure signals before any macroscopic movement could indicate impending failure in fast to very fast landslides, showing their potential to be used in EWS. Validation of estimated velocities was not always possible due to PIV setup constraints and the velocity of the mass movement simulated. In fact, the estimated translational velocities seem to be unreliable. On the other hand, the results suggest that acceleration data and angular position variation trend and rate can be incorporated into EWS.

1. Introduction

Landslide disaster prevention involves forecasting landslides enough time in advance to allow for actions to be taken towards reducing the possible damages. This prediction can be made in spatial or temporal terms (Intrieri et al., 2019). A spatial prediction relates the distribution of previous and potential landslides with the frequency of those events in the past. One of the most important products of this type of prediction for disaster prevention is the susceptibility maps, developed with computational models, such as SHALSTAB, TRIGRS, among others, as in Melo et al. (2021) and Craig & Augusto Filho (2020).

A temporal prediction is related to time of failure determination methods. For a regional scale prediction, rainfall monitoring is commonly used, as in Bandeira & Coutinho (2015), whereas slope scale prediction focuses on geotechnical instrumentation monitoring. As stated by Intrieri et al. (2019), a traditional and reliable approach for

landslide early warning is to monitor slope displacement and to analyze its derivatives (velocity and acceleration). The most used method to forecast the time of failure was developed by Fukuzono (1985), who defined a linear relationship between the time of failure and the inverse of velocity: failure moment can be inferred when that value approximates to zero. This method has been largely applied as detailed by Intrieri et al. (2019).

Regarding the monitoring issue, Yin et al. (2010), Stähli et al. (2015) and Askarinejad & Springman (2017) emphasized the need of using remote real time, high resolution and automatized sensors, considering failure can happen at high speed and pre-failure signals can be measured only a short time before rupture. Askarinejad et al. (2018) identified previous signals in a real scale landslide simulation experiment 2.5 h before failure happened (accelerating increase of horizontal pressure) and more significantly 23 min before failure for surface displacements and 30 min before for subsurface deformations. Because the precursors detection

depends on the measurement resolution and the type of the employed sensors, as well as on the triggering mechanism and the material type, it is important to perform experiments in controlled conditions to analyze whether monitoring sensors can identify pre-failure signals with sufficient time for actions to be taken.

In this sense, accelerometers are promising devices for landslide early detection. Technological developments have allowed manufacturing these sensors at lower costs allowing remote monitoring. Previous papers describe the use of accelerometers for landslide precursor detection and characterization purposes, such as Arnhardt et al. (2007), Azzam et al. (2010), De Dios et al. (2009), Segalini & Carini (2013), Ooi et al. (2014), Uchimura et al. (2015), Khoa et al. (2017), Giri et al. (2018), Dikshit & Satyam (2019), Ruzza et al. (2020), Sheikh et al. (2021) and Towhata et al. (2021).

Arnhardt et al. (2007) and Azzam et al. (2010) suggest implementing accelerometers in a rockslide EWS, however, they do not present results from this instrumentation. De Dios et al. (2009) tested in laboratory conditions a column sensor built with triaxial accelerometers buried for slope tilt measurements, similar to those developed by Segalini & Carini (2013). Like Giri et al. (2018), Ooi et al. (2014) monitored soil movements with accelerometers associated with gyroscopes to measure translational and rotational components in landslides simulated in a flume. Giri et al. (2018) also proposed a criterion to establish slow and rapid translational landslides and identify failure types through sensor readings. Khoa et al. (2017) used experimentally triaxial accelerometers to calculate slope angles and classify three types of movement: collision, slide down and rolling down. Ruzza et al. (2020) developed a low-cost pipe for tilt measurements built with an arrangement of triaxial accelerometers, similar to De Dios et al. (2009) and Segalini & Carini (2013). The instrument performance was successfully checked in laboratory experiments.

Literature review suggests that there is no consensus yet on how to employ accelerometers for landslide monitoring. Some works focused on using accelerometers associated with other sensors to characterize landslides qualitatively and to better understand the movement itself, like Ooi et al. (2014), Khoa et al. (2017) and Giri et al. (2018), whereas other authors used accelerometers in a similar fashion as inclinometers (De Dios et al., 2009; Segalini & Carini, 2013; Ruzza et al., 2020). Uchimura et al. (2015) developed an EWS based on tiltmeters, which are, in principle, dampened accelerometers, and tilting variation, mostly being used in Asian countries recently, as in Dikshit & Satyam (2019), Sheikh et al. (2021) and Towhata et al. (2021).

These previous works confirmed that accelerometers are strong instruments for geotechnical monitoring, mainly to monitor changes in slope tilt and to qualify failure types. Since there is no consensus in how to deploy and use accelerometers, it is crucial to validate their use in laboratory conditions before deploying them in real conditions. This

has been accomplished in the research presented here by simulating landslides in a flume, similar to what was done by other researchers with different sensors (Fukuzono, 1985; Ooi et al., 2014; Uchimura et al., 2015; Giri et al., 2018; Franco et al., 2019).

The main objective of this paper is to disclose the results obtained using low-cost biaxial accelerometers to identify pre-failure signals in a landslide simulated in a small-scale tilting flume experiment, where failure was triggered by percolating water into sandy soil, in a 30º slope. The overall performance of the low-cost accelerometers in detecting failure precursors is presented and discussed.

2. Experimental setup

2.1 Landslide flume

In this research, the results from one landslide simulated using a flume are presented. The glass side of the flume allows soil observation during the experiments. The flume is 1.60 m long, 0.5 m wide and 0.5 m deep and can be tilted up to 45° with a hydraulic jack (Figure 1). Three sections, namely "Upper part", "Intermediate part" and "Lower part", are indicated in this figure. Those terms will be used in this paper to explain the position of the sensors during the experiments. However, there are no internal divisions in the flume.

A perforated water hose was deployed at the base of the flume, to allow water percolation at the base of the soil sample. The water hose was covered with geosynthetic in order to minimize internal soil erosion.
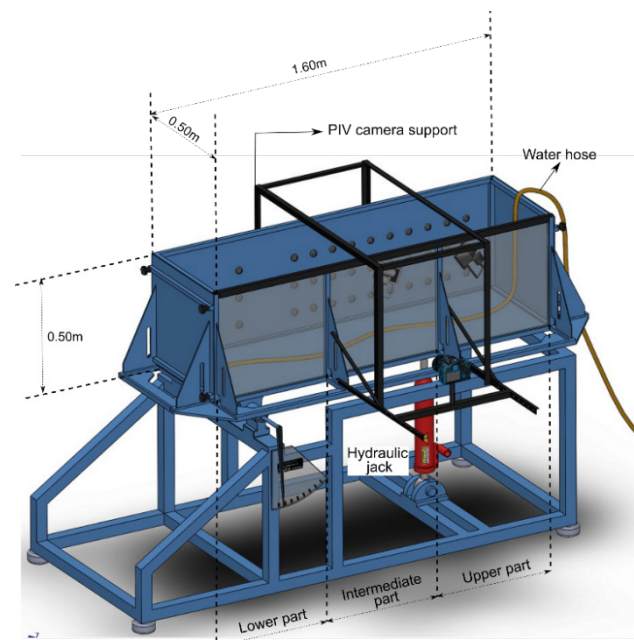

Figure 1. Tilting flume used for landslide simulation experiments and its components.

The soil used in this research is a uniform medium sand, with a mean particle diameter of 0.27 mm composed by 96% silica. Soil parameters are: $D_{10} = 0.16$ mm, $D_{30} = 0.22$ mm, $D_{60} = 0.30$ mm, $e_{max} = 0.92$, $e_{min} = 0.70$, $\gamma_{d,max} = 15.30$ kN/m³, $\gamma_{d,min} = 13.54$ kN/m³ and $G = 2.65$. According to the Unified Soil Classification System (USCS), the soil is classified as poorly graded sand, with uniformity coefficient of 1.90. The internal friction angle of soil is equal to 31º and cohesion is 0 kPa. They were determined using direct shear tests performed with dry soil and normal stresses ranging from 10 to 80 kPa. 30% of total dry soil volume was dyed with black waterproof ink (brand Indian Ink Talens), to enhance particle contrast for PIV analysis.

2.2 Landslide simulation experiment

The sample for the landslide simulation experiment was prepared according to the following steps:

1. The flume was filled in horizontal position with 0.3 m height of dry sandy soil, compacted with a wooden hammer in six layers at its maximum dry density;
2. Water supply was switched on to partially saturate the soil. The water supply was switched off when 75% of the soil's height (from bottom to top) was saturated;
3. A slope of 30º was excavated in the lower part of the flume;
4. Camera support was attached to the intermediate part;
5. The lowest door was opened, and the flume was tilted to 30°;
6. Water supply was brought back;
7. Acceleration data and picture acquisitions started simultaneously. This is considered time zero of the experiment (t = 0). During the experiment, the lowest

door was kept open, to allow soil to freely move down the flume. The experiment was performed at constant water flow of 4.4 L/min.

2.3 Instrumentation

Accelerometers were used for soil monitoring during the experiment. Five micro-electrical-mechanical-system (MEMS) accelerometers (ADXL-321, Analog Devices) were embedded into the soil during the model preparation phase. These accelerometers are biaxial (axes are called in this paper u and v). According to the manufacturer, their main characteristics are: measurement rate of +/- 18 g, bandwidth from 0 to 100 Hz and typical resolution values of 3 mg at 50 Hz. Accelerometers were encapsulated in aluminum alloy square boxes of 2.5 cm width and 1.0 cm height. Data were transmitted through 3 mm diameter flexible cables to a datalogger connected to a computer. Devices were positioned with the u axis parallel to the main movement direction and v perpendicular to u (Figure 2). Five accelerometers were embedded into the soil (numbers 1 to 5) and one accelerometer (number 6) was fixed on the external side of the steel wall. Therefore, accelerometer n. 6 was used as a benchmark of no soil movement.

2.4 PIV setup

The camera support is made of steel bars that can be bolted in the intermediate and upper parts and can be removed during sample preparation. Two LED reflectors are attached to the support and the room is darkened during the experiment, in order to keep the light supply constant. The camera used in this research is a Canon EOS Rebel T3i, with 18 MPx resolution, 35 mm of focal length, 1/5 s exposure time and maximum acquisition rate of 1 frame every 5 seconds.
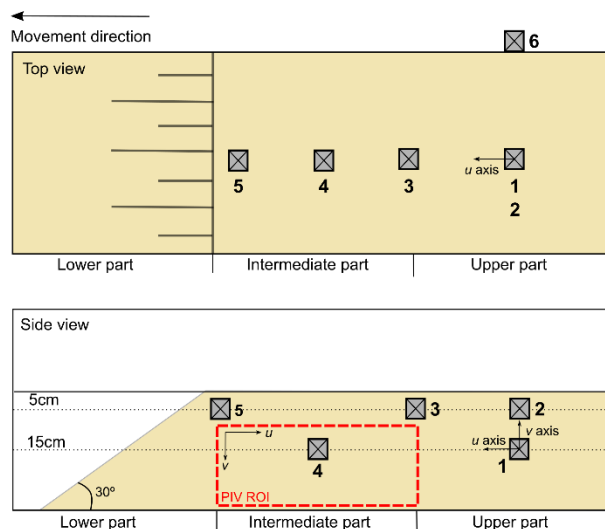

Figure 2. Sensors and PIV ROI positions during the experiment.

3. Data processing

3.1 Acceleration data processing procedure

Acceleration was measured in two directions and the resultant acceleration was calculated from those values. Analyzing resultant and components separately gives information about how the device moved during the experiment. Two types of movement can be identified by this analysis: in the first type, if the resultant acceleration remains constant with magnitude equals to 1 *g*, the gravity acceleration on Earth magnitude, it was assumed that no movement or negligible movement happened along the plane defined by accelerometer's *u* and *v* axes. In this case, although the resultant is constant, concomitant accelerations may happen in both components, indicating that the device had pitched. On the contrary, with decreasing resultant acceleration, it was considered that the device rotated around *u* or *v* axes, or achieved post-failure high acceleration translational movement. Therefore, focusing on the pre-failure period, it is considered that the device had rolled (rotated around *u*) or yawed (rotated around *v*).

Data were acquired at 4 kHz aiming to identify high frequency impulsive signal, which were supposed to be generated in crack formation, and also low frequency signal related to slow soil movement. First, raw data were analyzed for impulsive acceleration signals identification. After that, two Python routine codes were developed and employed to process accelerometer low frequency signal content and estimate landslide translational velocity from acceleration. The first one corresponds to filtering of acceleration data in time domain and aims to clear possible data outliers and high frequency noise. At this stage, a 4th order Butterworth filter was applied, with cutoff frequency of 1 Hz. Processed signals were analyzed for the identification of features that could be indicative of impending failure.

The second routine code was used to calculate the translational velocity from acceleration, by integrating the acceleration over time. Although it may seem like a simple procedure, it is necessary to admit that even when there is no soil movement, acceleration is measured. This acceleration is related to the Earth gravity acceleration projection on each accelerometer axis. Therefore, to calculate velocity, it was necessary to first remove gravity acceleration effects from measured accelerations. Hence, raw data were submitted to two processing steps: one to clear outliers, by using the same Butterworth filter aforementioned (the output of this step was called "filtered data") and another one for gravity offset removal, by applying a 10 s centralized window moving average filter on the "filtered data" (output of this step was called "smoothed data") and subtracting it from filtered data. Finally, the result was integrated to estimate the translational movement velocity.

To employ this translational velocity estimation procedure, it must be assumed that the small amplitude of the accelerometer's initial movement happened approximately along the plane defined by *u* and *v* axes. When failure happens, accelerometers can rotate about *u* and *v* and this assumption is no longer valid.

Angular position over time was also calculated from smoothed data accelerations in *u* and *v* directions, following Equations 1 and 2:

$$\theta_u = \frac{180 \cdot \arcsin\left(a_{us}\right)}{\pi} \quad (1)$$

$$\theta_v = \frac{180 \cdot \arccos\left(a_{vs}\right)}{\pi} \quad (2)$$

where θ_u and θ_v are estimations of the accelerometer angular position, in degrees, based on smoothed data accelerations a_{us} (in *u* direction) and a_{vs} (in *v* direction). Note that θ_u and θ_v are equal and correspond exactly to the accelerometer angular position if the plane defined by *u* and *v* axes is perfectly vertical and the accelerometer is at rest (behaving as an inclinometer).

3.2 PIV data processing procedure

The Particle Image Velocimetry (PIV) is a velocimetry technique developed for experimental fluid mechanics, using double-flash photography of a seeded flow (Adrian, 1991). According to Take (2015), from the late 1990s onwards researchers became aware that this technique was also well-suited for geotechnical engineering applications. Many geotechnical processes such as collapse of shallow foundations or landslides triggering involve granular flow and can, therefore, take advantage of the technique.

Since then, PIV has been widely used in laboratory experiments (Take et al., 2004; Baba & Peth, 2012; Franco et al., 2019) or in field experiments (Akca 2013; Askarinejad et al., 2018). Previous works show that results from PIV technique are similar to those achieved with in situ instruments. Although the values are not exactly the same, good agreement in order of magnitude and rates of change is observed (Askarinejad, 2013; Pei et al., 2019).

In this research, PIV Lab®, a free Matlab tool, developed by Thielicke (2020), was used for PIV analysis. Figure 2 shows the region of interest (ROI) defined to perform the analysis in experiment. Before choosing this ROI, some tests were performed with different ROI sizes. However, the results did not show any significant difference.

4. Results

4.1 Soil movement and acceleration results

Figure 3 shows schematically and illustrates with pictures the main experiment events. Landslide happened in a unique event, although a soil block developed during the experiment, but
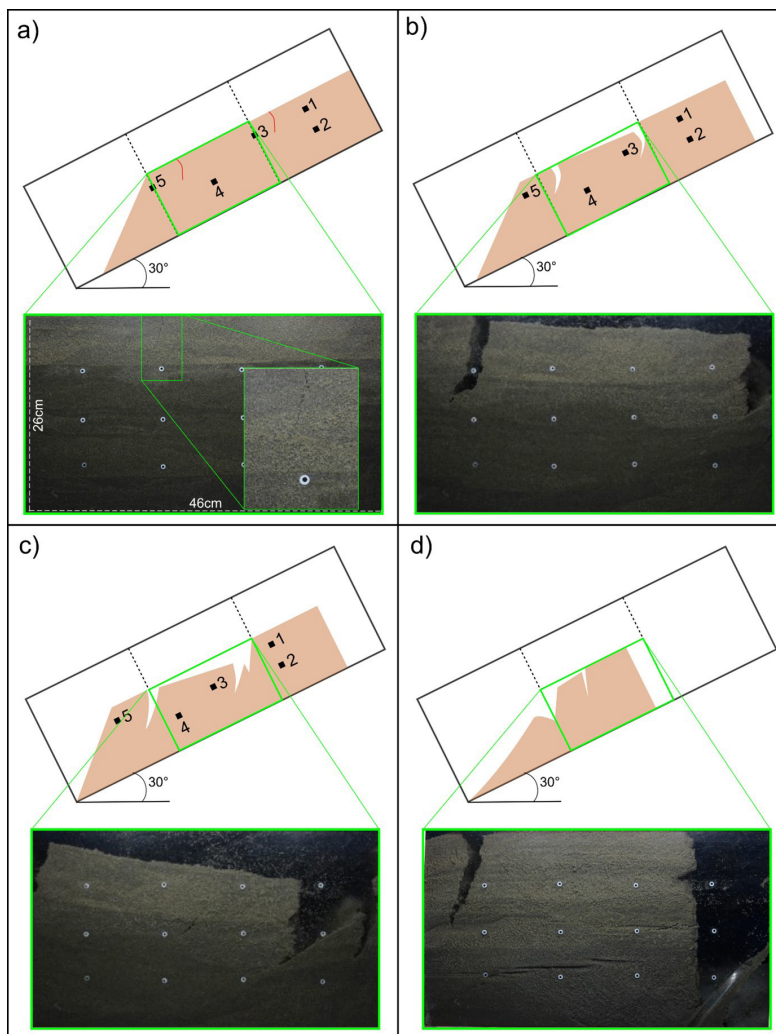
Figure 3. Schematic movement evolution during experiment: (a) time = 5 s: cracks started to develop in the intermediate part, defining a block; (b) time = 45 s: block started to move forward; (c) time = 65 s: block stopped moving and remained in the same position until failure; (d) time = 81 s: end of the experiment, all accelerometers fell out of the flume. Pictures were taken in the intermediate part of the flume.

remained in the same position until general failure happened. At 5 s, cracks started to develop in the intermediate part, defining a block (Figure 3a) where accelerometers n. 3 and n. 4 were embedded. From 45 s to 65 s (Figure 3b and Figure 3c), the block moved and remained in that position until failure happened at 81 s (Figure 3d). At the end of the experiment, part of the soil and all accelerometers fell out of the flume.

Figures 4 and 5 show the experiment acceleration results in u and v directions respectively and Figure 6 presents the calculated resultant acceleration. Benchmark acceleration is shown in black.

The collected acceleration data were primarily analyzed for the identification of impulsive signal features. Since none of such features could be detected, acceleration results presented in this section focus on low frequency content of those signals. Table 1 summarizes the results achieved with the five accelerometers embedded in the soil.

Figure 4. Acceleration results: filtered acceleration component in u direction for accelerometers n. 1 (red), n. 2 (magenta), n. 3 (cyan), n. 4 (blue), n. 5 (green) and n. 6 (benchmark, black). Block detachment and macroscopic failure are highlighted.

Table 1. Summary of acceleration variation and angular responses.

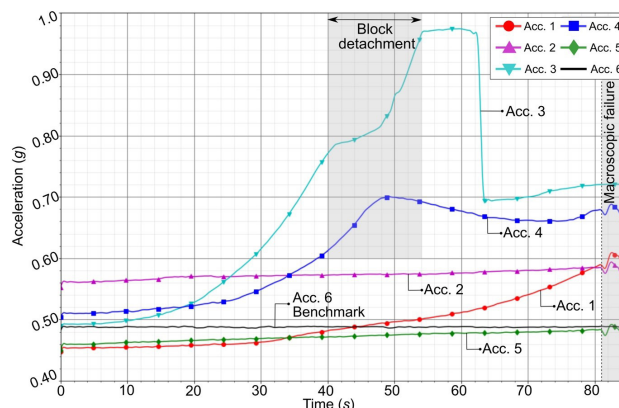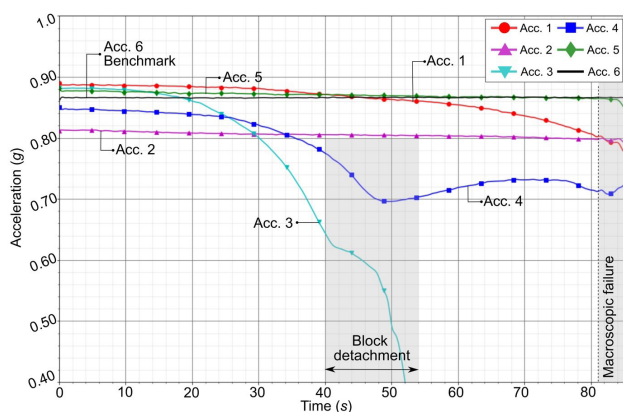| Acc.	Failure or Block detachment time (s)	Acceleration variation start time in component (s)	Difference in time between failure and first signal (s)	Acceleration variation (g)		Angular variation (º)	
				u direction	v direction	u direction	v direction
1	81	5	66	0.130	0.082	9	9
2	81	15	76	0.022	0.014	1.5	1.5
3	45	5	40	0.260	0.290	20	20
4	45	5	40	0.200	0.150	13	13
5	81	5	76	0.025	0.010	1.5	1.5

Figure 5. Acceleration results: filtered acceleration component in v direction for accelerometers n. 1 (red), n. 2 (magenta), n. 3 (cyan), n. 4 (blue), n. 5 (green) and n. 6 (benchmark, black). Block detachment and macroscopic failure are highlighted.
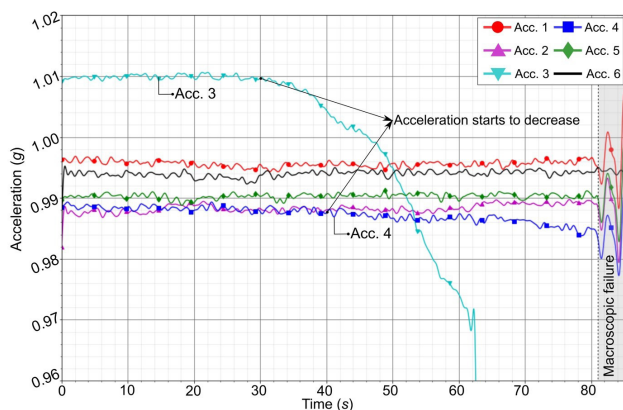
Figure 6. Resultant acceleration calculated for accelerometers n. 1 (red), n. 2 (magenta), n. 3 (cyan), n. 4 (blue), n. 5 (green) and n.6 (benchmark, black). Macroscopic failure is highlighted.

As it can be seen in Figure 4 and Figure 5, all accelerometers experienced acceleration variation in both directions before macroscopic failure happened, in agreement with macroscopic observations. Table 1 shows the time when each device measured acceleration variation and also the magnitude of acceleration variations.

Accelerometers n. 1, n. 2 and n. 5 presented a similar behavior: acceleration started to increase in u direction and decrease in v direction until macroscopic failure happened. Accelerometers n. 1 and n. 5 started to identify this behavior at 5 s whilst accelerometer n. 2, at 15 s, indicating that from this time onwards accelerometers started to pitch. Accelerometer n. 1 presented variation at $10^{-1}\,g$, whilst accelerometers n. 2 and n. 5 at $10^{-2}\,g$.

Accelerometers n. 3 and n. 4, located in the intermediate part of the flume, also identified acceleration variation related to block detachment. Both accelerometers started to measure acceleration variation at 5 s, indicating pitching movement, that was more pronounced between 40 s and 55 s, when block detachment happened. Resultant acceleration variation observed in both accelerometers is related to block detachment and indicates rolling or yawning movements because resultant acceleration decreased. After 60 s and before macroscopic failure happened, at 81 s, both accelerometers experienced deceleration, suggesting that deceleration do not necessarily imply in stabilization. Accelerometers n. 3 and n. 4 presented variation at $10^{-1}\,g$.

Resultant accelerations showed in Figure 6 indicate that accelerometers n. 3 and n. 4 experienced rotation (rolling or yawning) from 30 s and 40 s onwards respectively whereas the other accelerometer's resultant acceleration remained constant at 1 g, suggesting that those sensors did not rotate about u or v directions until failure happened at 81 s.

4.2 Translational velocity estimation

PIV analysis was run with PIV Lab® Matlab tool. The tool compares subsequent images from the same ROI and tracks the same pixels in each image to calculate velocity during the time elapsed between those images. The first pair of images that was analyzed are images from 0 s and 5 s. Hence, the result obtained from those images is considered the velocity calculated at t = 5 s. In cases where it is not possible to find the same pixel, velocity vectors are interpolated from surrounding information.

In this research, velocity up to 30 s of the experiment was calculated, as can be seen in Figure 7. From this time onwards analysis was considered unreliable since the quantity of interpolated vectors increased significantly as a result of the low picture acquisition rate. Also, estimated velocity remained constant which is not consistent with the movement observed. Up to 30 s, PIV calculated velocities ranged from 6.0×10^{-4} to
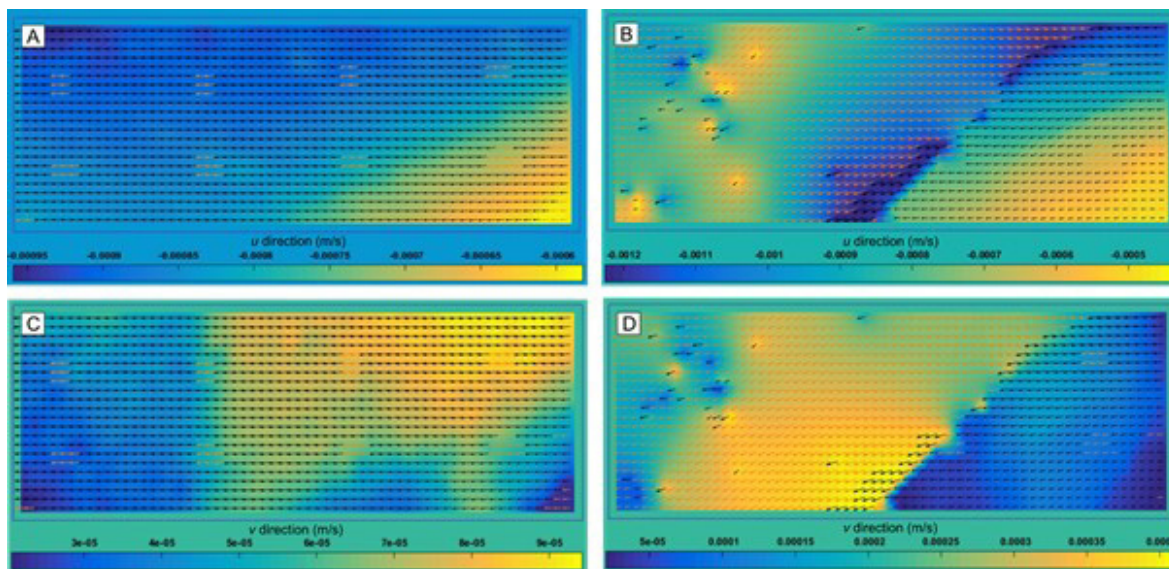
6

Otero et al., Soil. Rocks, São Paulo, 2022 45(3):e2022078621

Figure 7. PIV Lab graphics output for *u* (A and B) and *v* directions (C and D). Figures A and C are for t=5 s and B and D for t=30 s.

1.2×10^{-3} m/s in *u* direction and from 3.0×10^{-5} to 4.0×10^{-4} m/s in *v* direction. This reveals that the simulated landslides were rapid to very rapid according to Hungr et al. (2014).

Unfortunately, translational velocities calculated from accelerometers data resulted in inconsistent results compared to those obtained using the PIV method. Moreover, the benchmark accelerometer remained still during the tests, but the processing procedure estimated velocity fluctuations between 0 and 10^{-3} m/s, although the mean value consistently remained around zero for this sensor. These aspects revealed that the data processing presented in Section 3 did not remove completely the gravity effects on moving accelerometers, probably due to a correlation between translational and rotational movements (and similarity in their frequency content), and to the accelerometer sensitivity to external noise being too high concerning velocity quantification. Nevertheless, the angular position calculation procedure was robust, as presented below.

4.3 Angular position variation in time

Figure 8 shows the angular position variation calculated, which is also presented for each accelerometer in Table 1. Results indicate that angular position started to change before block detachment and general failure happened, showing similar results to those of acceleration trends. Because the magnitude of the angle variation is the same for both axes, only the results of *u* direction angle position are presented.

The angular variation results corroborate the results observed with the acceleration variation: the devices measured angular variations that indicate progressive microscopic movements, although at macroscopic scale no remarkable observations could be made for the same time intervals.

Previous works, such as Ooi et al. (2014), Khoa et al. (2017) and Giri et al. (2018), used this angular variation to
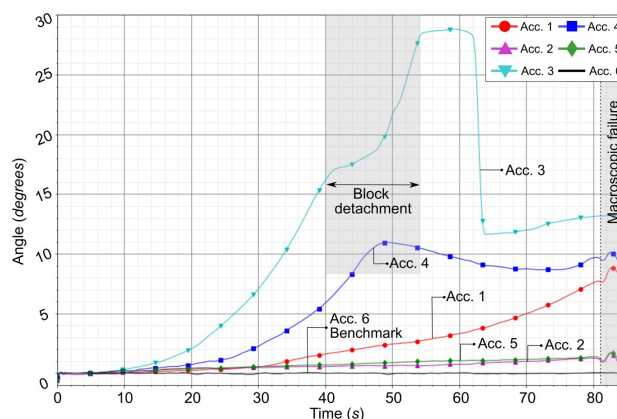

Figure 8. Angle variation calculated for accelerometers n. 1 (red), n. 2 (magenta), n. 3 (cyan), n. 4 (blue), n. 5 (green) and n. 6 (benchmark, black). Macroscopic failure and block detachment are highlighted.

qualitatively define the type of soil movement. By analyzing how angular variation occurred, together with other sensors, they indicate if the movement was rotational or translational. However, they did not focus their research on evaluating if the sensors were able to measure variations before rupture happened.

5. Discussion

A traditional approach for landslide early warning is to monitor slope deformations and to analyze movement velocity increase, as defined by Fukuzono (1985). Xu et al. (2011) calculated soil velocity and acceleration based on displacement data, proposing a criterion to analyze acceleration increase and establish acceleration threshold values for the development of an EWS.

This research aimed at measuring the acceleration directly, although it was not possible to identify resultant acceleration increase in any sensor during the pre-failure period. As explained in the previous section, velocities calculated from acceleration measurements were not consistent compared to those obtained based on PIV method, indicating that the data processing procedure did not succeed in terms of gravity offset removal. As gravity acceleration is many orders of magnitude higher than the movement acceleration, this could not be quantified. This implies that the proposed measuring and processing method is not capable of indicating an increase in acceleration in the same sense as Xu et al. (2011).

Nevertheless, when analyzing u and v components separately, in all cases, acceleration variations can be interpreted as pre-failure signals. Those signals measured in each component are related to small scale movement rather than to the macroscopic failure movement and they imply that the sensors are pitching prior to macroscopic failure. Macroscopically, it is not always possible to observe the whole soil massif moving, however, movement is happening in particle scale and accelerometers were able to capture these movements.

Different acceleration trends observed in each device confirm that, for slope monitoring, it is highly important to work with a sensor network, since different parts of the slope may have different behaviors. The importance of monitoring networks has been demonstrated by Arnhardt et al. (2007), Azzam et al. (2010), Ramesh (2014), Li et al. (2016), Giordan et al. (2019), among others.

Furthermore, it was observed that at particle scale the soil may experience rotation (pitching), even though at macroscopic scale the movement was a translational landslide. This indicates that an Inertial Measurement Unit (IMU) could be used in order to detect both translational and rotational movements. On the other hand, IMU's long-term stability and energy consumption are factors to be considered.

The angular variation observed in the experiment has a progressive growth trend, which predates the landslide and can be interpreted in a similar way as proposed by Fukuzono (1985) for translational velocity. This is in line with the early warning proposal made by Uchimura et al. (2015) and that has been used recently in Asian countries (Dikshit & Satyam, 2019; Xie et al., 2020; Towhata et al., 2021; Sheikh et al., 2021).

6. Conclusions

In this research, landslide was simulated in a tilting flume, where movement was triggered by tilting the slope and percolating water into the soil. To monitor soil behavior during the experiment, five low-cost accelerometers were embedded into the soil and images were acquired with an external camera.

By analyzing acceleration data, it became clear that accelerometers measured acceleration variations in each component that can be interpreted as pre-failure signals which indicate that, at particle scale, pitching happened, although no macroscopic displacement observations were made. In some cases, pre-failure signals were measured more than one minute before failure.

The well-established procedure to estimate time of failure from translational velocity variation in time could not be used in this case, because the procedure to estimate translational velocity from acceleration data did not work properly. This likely happened due to a correlation between rotational and translational movements of the accelerometers, leading to a similarity in their frequency contents that precluded gravity effect removal by the proposed processing procedure based on traditional filtering procedures.

Nevertheless, even using low-cost biaxial accelerometers, it was possible to quantify the angular variation during the experiment. The results suggest that angle variations can be interpreted as pre-failure signals and that landslides EWS could be based directly on acceleration data or on angular position variation trends and rates.

Since no impulsive features were detected and landslide movement happened at very low frequencies, in future research or in field deployments it is not necessary to acquire data at such high rates, as done in this research. Sensor resolution and noise sensibility were also issues concerning velocities quantification. However, improving sensor characteristics implies using more expensive accelerometers and the scope of the research was to test low-cost sensors, economically viable for large area monitoring.

For future works, it is important to test the accelerometers responses in slower movements. It is expected that in field conditions, impending failure signals may be identified earlier than in this research. The use of triaxial sensors is recommended in order to measure yawning and rolling movements.

Acknowledgements

Declaration of interest

The authors have no conflicts of interest to declare. All co-authors have observed and affirmed the contents of the paper and there is no financial interest to report.

Authors' contributions

Malena D'Elia Otero: data curation, investigation, methodology, visualization, writing - original draft. Ana Elisa Silva de Abreu: conceptualization, supervision, writing

List of symbols

D_{10}	effective grain size
D_{30}	sieve size through which 30% (by weight) of the material passes
D_{60}	sieve size through which 60% (by weight) of the material passes
e_{max}	maximum void index
e_{min}	minimum void index
$\gamma_{d,max}$	maximum dry unit weight
$\gamma_{d,min}$	minimum dry unit weight
G	density of solids
u	accelerometer axis parallel to movement main direction
v	accelerometer axis perpendicular to movement main direction
a_{us}	smoothed acceleration calculated in u direction
a_{vs}	smoothed acceleration calculated in v direction
θ_u	accelerometer angular position estimated in u direction
θ_v	accelerometer angular position estimated in v direction

References

Adrian, R.J. (1991). Particle-imaging techniques for experimental fluid-mechanics. *Annual Review of Fluid Mechanics*, 23(1), 261-304. http://dx.doi.org/10.1146/annurev.fl.23.010191.001401.

Akca, D. (2013). Photogrammetric monitoring of an artificially generated shallow landslide. *The Photogrammetric Record*, 28(142), 178-195. http://dx.doi.org/10.1111/phor.12016.

Arnhardt, C., Asch, K., Azzam, R., Bill, R., Fernández-Steeger, T.M., Homfeld, S., Kallash, A., Niemeyer, F., Ritter, H., Toloczyki, M., & Walter, K. (2007). Sensor Based Landslide Early Warning System - SLEWS: development of a geoservice infrastructure as basis for early warning systems for landslides by integration of real-time sensors. In *Early Warning Systems in Earth Management: Kick-Off-Meeting* (pp. 75-88). Technical University Karlsruhe.

Askarinejad, A., & Springman, S.M. (2017). A novel technique to monitor subsurface movements of landslides. *Canadian Geotechnical Journal*, 55(5), 620-630. http://dx.doi.org/10.1139/cgj-2016-0338.

Askarinejad, A. (2013). *Failure mechanisms in unsaturated silty sand slopes triggered by rainfall* [D.Sc. thesis]. ETH Zurich.

Askarinejad, A., Akca, D., & Springman, S.M. (2018). Precursors of instability in a natural slope due to rainfall: a full-scale experiment. *Landslides*, 15(9), 1745-1759. http://dx.doi.org/10.1007/s10346-018-0994-0.

Azzam, R., Arnhardt, C., & Fernández-Steeger, T.M. (2010). Monitoring and early warning of slope instabilities and deformations by sensor fusion in self-organized wireless ad-hoc sensor networks. *Journal of Southeast Asian Applied Geology*, 2(3), 163-169.

Baba, H.O., & Peth, S. (2012). Large scale soil box test to investigate soil deformation and creep movement on slopes by Particle Image Velocimetry (PIV). *Soil & Tillage Research*, 125, 38-43. http://dx.doi.org/10.1016/j.still.2012.05.021.

Bandeira, A.P.N., & Coutinho, R.Q. (2015). Critical rainfall parameters: proposed landslide warning system for the Metropolitan Region of Recife, PE, Brazil. *Soils and Rocks*, 38(1), 27-48. http://dx.doi.org/10.28927/SR.381027.

Craig, A.M.L., & Augusto Filho, O. (2020). Landslide susceptibility mapping of highway slopes, using stability analyses and GIS methods. *Soils and Rocks*, 43(1), 71-84. http://dx.doi.org/10.28927/SR.431071.

De Dios, J.C., Enriquez, J., Victorino, F.G., Mendoza, E.A., Talampas, M.C., & Marciano, J.J. (2009). Design, development and evaluation of a tilt and moisture sensor network for slope monitoring applications. In *TENCON 2009-2009 IEEE Region 10 Conference* (pp. 1-6), Singapore.

Dikshit, A., & Satyam, N. (2019). Probabilistic rainfall thresholds in Chibo, India: estimation and validation using monitoring system. *Journal of Mountain Science*, 16(4), 870-883. http://dx.doi.org/10.1007/s11629-018-5189-6.

Franco, Y.B., Silva, J.L., & Valentin, C. (2019). A new small-scale test apparatus for modeling buried pipes under axial or lateral soil loading. *Geotechnical Testing Journal*, 43(1), 20180228. http://dx.doi.org/10.1520/GTJ20180228.

Fukuzono, T.A. (1985). A new method for predicting the failure time of a slope. In *Proceedings of the Fourth International Conference and Field Workshop on Landslides* (pp. 145-150). Tokyo: Landslides Society.

Giordan, D., Wrzesniak, A., & Allasia, P. (2019). The importance of a dedicated monitoring solution and communication strategy for an effective management of a complex active landslides in urbanized areas. *Sustainability*, 11, 946. http://dx.doi.org/10.3390/su11040946.

Giri, P., Ng, K., & Phillips, W. (2018). Laboratory simulation to understand translational soil slides and establish movement criteria using wireless IMU sensors. *Landslides*, 15(12), 2437-2447. http://dx.doi.org/10.1007/s10346-018-1055-4.

Hungr, O., Leroueil, S., & Picarelli, L. (2014). The Varnes classification of landslide types, an update. *Landslides*, 11(2), 167-194. http://dx.doi.org/10.1007/s10346-013-0436-y.

Intrieri, E., Carlà, T., & Gigli, G. (2019). Forecasting the time of failure of landslides at slope-scale: a literature review. *Earth-Science Reviews*, 193, 333-349. http://dx.doi.org/10.1016/j.earscirev.2019.03.019.

Khoa, V.V., Nakano, T., Masanori, H., & Takayama, S. (2017). Detection of landslide disaster by telemetric sensing node network system. In *Proceedings of 11th Asian Control Conference (ASCC)* (pp. 447-452), Gold Coast, QLD, Australia.

Li, C., Azzam, R., & Fernández-Steeger, T.M. (2016). Kalman filters in geotechnical monitoring of ground subsidence using data from MEMS sensors. *Sensors*, 16(7), 1109-1123. http://dx.doi.org/10.3390/s16071109.

Melo, C.R., Guedes, P.A., Amorim, S.F., Alves, F.H.B., & Cirilo, J.A. (2021). Combined analysis of landslide susceptibility and soil water dynamics in a metropolitan area, northeast, Brazil. *Soils and Rocks*, 44(2), e2021051420. http://dx.doi.org/10.28927/SR.2021.051420.

Ooi, G.L., Wang, Y., Tan, P.S., So, C.F., Leung, M.L., Li, X., & Lok, K.H. (2014). An instrumented flume to characterize the initiation features of flow landslides. *Geotechnical Testing Journal*, 37(5), 1-21. http://dx.doi.org/10.1520/GTJ20130158.

Pei, H., Zhang, S., Borana, L., Zhao, Y., & Yin, J. (2019). Slope stability analysis based on real-time displacement measurements. *Measurement*, 131, 686-693. http://dx.doi.org/10.1016/j.measurement.2018.09.019.

Ramesh, M.V. (2014). Design, development, and deployment of a wireless sensor network for detection landslides. *Ad Hoc Networks*, 13, 2-18. http://dx.doi.org/10.1016/j.adhoc.2012.09.002.

Ruzza, G., Guerriero, L., Revellino, P., & Guadagno, F.M. (2020). A multi-module fixed inclinometer for continuous monitoring of landslides: design, development and laboratory testing. *Sensors*, 20(11), 3318. http://dx.doi.org/10.3390/s20113318.

Segalini, A., & Carini, C. (2013). Underground landslide displacement monitoring: a new MEMS based device. In C. Margottini, P. Canuti & K. Sassa (Eds.), *Landslide science and practice* (Vol. 2: Early warning, instrumentation and monitoring, pp. 87-93). Berlin: Springer. http://dx.doi.org/10.1007/978-3-642-31445-2_11.

Sheikh, M.R., Nakata, Y., Shitano, M., & Kaneko, M. (2021). Rainfall-induced unstable slope monitoring and early warning through tilt sensors. *Soil and Foundation*, 61(4), 1033-1053. http://dx.doi.org/10.1016/j.sandf.2021.05.010.

Stähli, M., Sättele, M., Huggel, C., McArdell, B.W., Lehmann, P., van Herwijnen, A., Berne, A., Schleiss, M., Ferrari, A., Kos, A., Or, D., & Springman, S.M. (2015). Monitoring and prediction in early warning systems for rapid mass movements. *Natural Hazards and Earth System Sciences*, 15(4), 905-917. http://dx.doi.org/10.5194/nhess-15-905-2015.

Take, W.A. (2015). Thirty-six Canadian Geotechnical Colloquium: advances in visualization of geotechnical processes through digital image correlation. *Canadian Geotechnical Journal*, 52, 1199-1220. https://doi.org/10.1139/cgj-2014-0080.

Take, W.A., Bolton, M.D., Wong, P.C.P., & Yeung, F.J. (2004). Evaluation of landslide triggering mechanisms in model fill slopes. *Landslides*, 1(3), 173-184. http://dx.doi.org/10.1007/s10346-004-0025-1.

Thielicke, W. (2020). *PIVlab: particle image velocimetry (PIV) tool.* Retrieved in December 14, 2021, from https://www.mathworks.com/matlabcentral/fileexchange/27659-pivlab-particle-image-velocimetry-piv-tool

Towhata, I., Goto, S., Goto, S., Akima, T., Tanaka, J., Uchimura, T., Wang, G., Yamaguchi, H., & Aoyama, S. (2021). Mechanism and future risk of slope instability induced by extreme rainfall event in Izu Oshima Island, Japan. *Natural Hazards*, 105(1), 501-530. http://dx.doi.org/10.1007/s11069-020-04321-0.

Uchimura, T., Towhata, I., Wang, L., Nishie, S., Yamaguchi, H., Seko, I., & Qiao, J. (2015). Precaution and early warning surface failure of slopes by using tilt sensors. *Soil and Foundation*, 22(5), 1086-1099. http://dx.doi.org/10.1016/j.sandf.2015.09.010.

Xie, J., Uchimura, T., Wang, G., Shen, Q., Maqsood, Z., Xie, C., Liu, J., Lei, W., Tao, S., Chen, P., Dong, H., Mei, G., & Qiao, S. (2020). A new prediction method for the occurrence of landslides based on the time history of tilting of the slope surface. *Landslides*, 17(2), 301-312. http://dx.doi.org/10.1007/s10346-019-01283-8.

Xu, Q., Yuan, Y., Zeng, Y.P., & Hack, R. (2011). Some new pre-warning criteria for creep slope failure. *Science China. Technological Sciences*, 54(S1), 210-220. http://dx.doi.org/10.1007/s11431-011-4640-5.

Yin, Y., Wang, H., Gao, Y., & Li, X. (2010). Real-time monitoring and early warning of landslides at relocated Wushan Town, the Three Gorges Reservoir, China. *Landslides*, 7(3), 339-349. http://dx.doi.org/10.1007/s10346-010-0220-1.